AFRL-SR-BL-TR-98-

0363

REPORT DOCUMENTATION PAGE

1. AGENCY USE ONLY (Leave blank)	2. REPORT DATE	3. REPORT TYPE AND DATES COVERED
	3 April 1998	Final Technical Report 3/1/95 – 2/28/98

4. TITLE AND SUBTITLE

(U) Rapid Concentration Measurements by Picosecond Time-Resolved Laser-Induced Fluorescence

5. FUNDING NUMBERS

PE – 61102F
PR –2308
SA – BS
G – F49620-95-1-0218

6. AUTHOR(S)

G. B. King and N. M. Laurendeau

7. PERFORMING ORGANIZATION NAME(S) AND ADDRESS(ES)

Purdue University
West Lafayette, IN 47907-1288

8. PERFORMING ORGANIZATION REPORT NUMBER

9. SPONSORING / MONITORING AGENCY NAME(S) AND ADDRESS(ES)

AFOSR/NA
110 Duncan Avenue, Suite B115
Bolling AFB DC 20332-0001

10. SPONSORING / MONITORING AGENCY REPORT NUMBER

19980430 084

11. SUPPLEMENTARY NOTES

12a. DISTRIBUTION / AVAILABILITY STATEMENT

Approved for public release; distribution is unlimited.

12b. DISTRIBUTION CODE

13. ABSTRACT *(Maximum 200 Words)* Quantitative measurements of scalars in combustion are crucial to our understanding of flame structure and pollutant production. Progress has been made in quantitatively characterizing many laminar flames; however, the inherent fluctuations in turbulent flames significantly complicate such measurements. Picosecond time-resolved laser-induced fluorescence (PITLIF) is a developing technique which seeks to provide the first known means of obtaining quantitative minor-species concentrations in flames at rates sufficient for the study of turbulent fluctuations. This method was developed and applied to measurements of sodium and OH concentrations in laminar flames under previous AFOSR funding. The present report details the construction of a second generation PITLIF instrument. The primary goal of this work is to provide a continuous time series of quantitative concentrations from which frequency domain statistics such as the power spectral density (PSD) can be computed. Using the new laser system, fluorescence measurements of CH and OH time series were collected in a variety of methane and hydrogen flames including nonpremixed turbulent flames. These data have also been compared with available velocity and temperature measurements. The time series and resulting PSDs represent the first measurements of these statistics for minor-species concentrations.

14. SUBJECT TERMS

Laser-Induced Fluorescence
Time-Resolved Fluorescence
Concentration Measurements
Turbulent Flames

15. NUMBER OF PAGES 26

16. PRICE CODE

17. SECURITY CLASSIFICATION OF REPORT	18. SECURITY CLASSIFICATION OF THIS PAGE	19. SECURITY CLASSIFICATION OF ABSTRACT	20. LIMITATION OF ABSTRACT
Unclassified	Unclassified	Unclassified	UL

Rapid Concentration Measurements by Picosecond Time-Resolved Laser-Induced Fluorescence

Final Report
Air Force Office of Scientific Research
Grant No. F49620-95-1-0218
March 1, 1995 - February 28, 1998

Galen B. King and Normand M. Laurendeau
School of Mechanical Engineering
Purdue University
West Lafayette, IN 47097-1288

ABSTRACT

Quantitative measurements of scalars in combustion are crucial to our understanding of flame structure and pollutant production. Progress has been made in quantitatively characterizing many laminar flames; however, the inherent fluctuations in turbulent flames significantly complicate such measurements. Picosecond time-resolved laser-induced fluorescence (PITLIF) is a developing technique which seeks to provide the first known means of obtaining quantitative minor-species concentrations in flames at rates sufficient for the study of turbulent fluctuations. This method was developed and applied to measurements of sodium and OH concentrations in laminar flames under previous AFOSR funding. The present report details the construction of a second generation PITLIF instrument. The primary goal of this work is to provide a continuous time series of quantitative concentrations from which frequency domain statistics such as the power spectral density (PSD) can be computed. Using the new laser system, fluorescence measurements of CH and OH time series were collected in a variety of methane and hydrogen flames including nonpremixed turbulent flames. These data have also been compared with available velocity and temperature measurements. The time series and resulting PSDs represent the first measurements of these statistics for minor-species concentrations.

1 RESEARCH OBJECTIVES

Measurements of radical concentrations in flames are required to understand many important interactions between fluid mixing and chemical reaction [1]. Advances in laser-based techniques have enabled nonperturbing, quantitative measurements of such species concentrations. In particular, laser-induced fluorescence (LIF) possesses the spatial and temporal resolution necessary to monitor radical concentrations in reacting flows. However, typical LIF measurements depend on the local quenching environment, thus complicating quantitative interpretation of the fluorescence data. Picosecond time-resolved laser-induced fluorescence (PITLIF) has been developed to address this problem. The PITLIF technique permits direct interrogation of both the integrated fluorescence signal (low-bandwidth) and the fluorescence lifetime (high-bandwidth). Measurement of the electronic quenching rate coefficient (Q_e) allows the evaluation of quantitative number densities from corrected fluorescence measurements [2]. Previous work has demonstrated the ability to measure both Q_e and the integrated fluorescence signal for a naturally-occurring minor species (OH) [3] and for a seeded substance (sodium) [2] in laminar flames. However, in a fluctuating environment (such as a turbulent flame), these measurements must be made simultaneously and very rapidly, as the concentration must be resolved at the smallest time scales of the flow. The instrumentation used in previous PITLIF experiments utilized separate pathways for the high- and low-bandwidth measurements; moreover, these results were not obtained simultaneously. Another limiting drawback to the previous instrumentation was its inherently low fluorescence signal (owing to the use of ten-year-old laser technology).

In the present report, we describe the construction of a new PITLIF instrument. This instrument uses a Ti:Sapphire laser system and provides as much as twenty times the signal achieved with the older Nd:YAG pumped dye-laser system. This increased signal permits, for the first time, time-series measurements of minor-species fluorescence. These time-series measurements are presented for CH and OH in laminar and turbulent diffusion flames. From these time series, the probability density function (PDF) and power spectral density (PSD) can be computed. The PDF can be measured using other techniques, but the PSD can only be found from a continuous time series, as provided with the PITLIF instrument. For nonreacting turbulent flows at high Reynolds numbers, the velocity PSD is known to exhibit a power law region at high frequencies with a slope of -5/3. The PSDs for CH and OH fluorescence are found to depart from this "expectation". On this basis, we examine some possible implications of the observed data.

2 RESEARCH ACCOMPLISHMENTS

2.1 Experimental Setup

A schematic diagram of the experimental apparatus is shown in Fig. 1. The laser source is a Spectra-Physics Tsunami^{TM} Ti:Sapphire, mode-locked laser which is pumped by a large-frame, multi-mode, argon-ion laser (20 W). The laser system delivers a series of mode-locked pulses of either 1.5 ps or 18 ps full-width at half-maximum (FWHM) at a repetition rate of 80 MHz. The pulse width is selected by interchanging an intracavity interferometer. The 1.5-ps output was utilized for CH measurements and the 18-ps output was utilized for OH measurements. The output of the Ti:Sapphire laser is frequency doubled with an angle-tuned

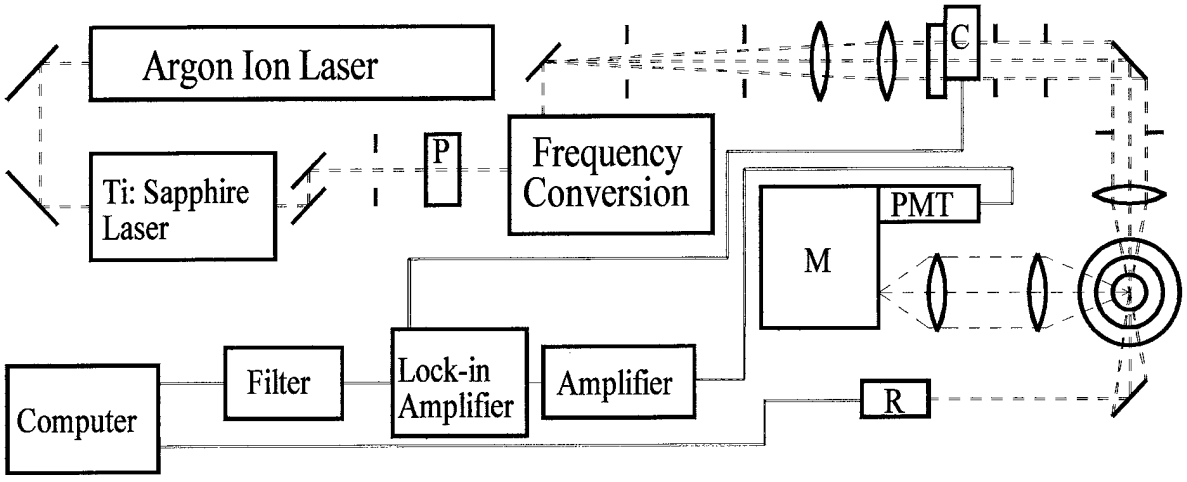

Figure 1. Experimental setup used for the time-series measurements of CH and OH: P, polarization rotator; C, chopper; M, 0.25-m monochromator; R, radiometer.

LBO crystal (for CH) and subsequently mixed with the residual fundamental with an angle-tuned BBO crystal to provide frequency tripling (for OH). The spectral width of the beam after being doubled is estimated to be 10 cm^{-1} (1.5-ps pulse) and after being tripled is approximately 1 cm^{-1} (18-ps pulse). The wavelength (~430 nm) and spectral width of the laser exiting the doubling crystal allows simultaneous excitation of 10-20 Q-branch transitions within the (0,0) band of the A^2-X^2 system of CH. The spectrally-narrower pulses (~1 cm^{-1}) from the 18-ps setting could be used, allowing excitation of a single rovibronic line, but significantly less laser energy is available owing to the reduced efficiency of the doubling process. This alternative strategy has been used to excite the temperature-insensitive $Q_1(10)$ line (Q_{1c} and Q_{2c}) of CH and has yielded similar results to those discussed here, but with a slightly lower signal-to-noise ratio (SNR). For OH, the wavelength was tuned to excite the relatively temperature-insensitive $Q_1(8)$ line in the (0,0) band of the A^2-X^2 system at 309.33 nm after frequency tripling. The beam diameter at the focus was measured to be ~100 μm FWHM for both laser settings.

Fluorescence was collected perpendicular to the laser beam with a 7.6-cm focal-length lens and focused into a 0.25-m monochromator via a 15.2-cm focal-length lens. The entrance slit of the monochromator (1 mm) was used, along with the beam diameter, to define the probe volume (100 μm × 100 μm × 500 μm). For OH, the exit slit of the monochromator (6.5 mm) was set to allow a detection bandwidth of 26 nm centered at 309 nm in the (0,0) band. For CH, the width of the exit slit was 1 mm, resulting in the detection of fluorescence in a 4-nm region centered at 430 nm. A PMT (Hamamatsu HS5321) with a risetime of 700 ps and a transit-time spread of 160 ps was used to detect the fluorescence. The PMT current was boosted by a low-noise preamplifier and then demodulated by a lock-in amplifier which utilizes phase sensitive amplification, tied to an optical chopper in the laser path, to increase the SNR. Typical lock-in amplifiers have a bandwidth of no more than 200 Hz. We have bypassed the 6-dB, internal filters of our lock-in system and have used an external, 8-pole, 6-zero, constant-delay, low-pass filter to provide analog signals with a bandwidth of over 10 kHz. This technique necessarily increases the noise, but is required to resolve the higher-frequency fluctuations in a turbulent flame. For the present measurements, the low-pass filter was set to provide a 2-kHz bandwidth owing to the 4-kHz operating limit for the optical chopper. A data acquisition board then sampled this signal at 4 kHz. Means, PDFs, and PSDs (0 - 2 kHz) were all computed from the sampled time series. These calculations comprise the major results presented in this report.

A concentric-tube burner was utilized for creating either a nonpremixed laminar or turbulent flame. Methane was supplied through a central tube (5.5-mm inner diameter). A stabilizing co-flow air stream was supplied to an outer tube (23.6-mm inner diameter) concentric to the central fuel tube. The air stream passed through glass beads and a honeycomb flow straightener and was used only with the laminar flame to dampen out any fluctuations caused by the movement of surrounding room air. The Reynolds number (based on the average velocity at the exit of the fuel tube) was 70 and 2,800 in the laminar and turbulent flames, respectively. The relatively low Reynolds number for the turbulent flame was required to ensure that the flame remained attached to the central fuel tube.

2.2 Quenching Corrections

Time-series measurements and on-the-fly quenching corrections are unique aspects of the PITLIF technique which permit monitoring transient events in real time. However, corrections via measurements of the CH or OH quenching rate coefficient have not been made to the present

data and may not be necessary for these particular flames. Studies of CH quenching cross-sections indicate that variations in Q_e should be minimal for the narrow region where CH is found to exist owing to a temperature-dependent cancellation between the total cross-section and the collision rate [4]. Thus, our uncorrected time-series measurements should represent the actual CH concentrations to within ~25% [5]. Likewise, variations in the quenching rate coefficient for OH in a laminar, methane/air, diffusion flame have been estimated previously at ±20% [6]. We have duplicated this numerical study by using more recent estimates of major species concentrations across the flame front [7] and the respective quenching cross-sections for OH as a function of temperature [8]. The results indicate that quenching variations should be no more than ±15% over the range of mixture fractions at which OH is experimentally found to exist (defined by $[OH] \geq 0.1[OH]_{max}$ based on the data of Barlow and Carter [9] and Smooke *et al.* [10]). This small variation in quenching enables a simplified technique for initial studies of the effects of turbulent combustion on minor-species concentrations. The development of a complete, on-the-fly quenching correction is part of the ongoing research for this project, as discussed in Section 3.

2.3 CH Fluorescence Measurements

To examine the temporal resolution of the current PITLIF system, time-series measurements of CH fluorescence signals were made in the pre-soot regions of both the laminar and turbulent nonpremixed flames. Local means and PSDs were then computed from these time series. Radial profiles of the mean CH signal at three different axial locations are shown for the laminar flame in Fig. 2. Since CH is only present in high-temperature regions of the flame, the displayed trends are to be expected. At all measurement locations, CH is present only near the flame front and drops off rapidly on either side of this location. Peak CH levels are highest at the lowest axial positions and decrease with height above the burner. Little or no CH is found in the cold, fuel-rich central core of the nonpremixed flame. Moreover, the symmetry of the radial profiles indicates that fluorescence trapping is not significant. Some Rayleigh scattering signal can be observed in the central region of the flame at x/D=1. This signal is insignificant in the high-temperature regions where CH is found owing to the inverse relationship of Rayleigh scattering to temperature. Of greater importance is the potential interference from polycyclic aromatic hydrocarbons (PAHs) that occurs just prior to the onset of soot. In particular, significant PAH emission is observed at and above x/D=3; however, at lower axial positions, PAH interferences are insignificant owing to the existence of a strong CH signal. Off-line profiles were also obtained (450-nm excitation), and the interferences from PAH and Rayleigh scattering were found to contribute less than 5% of the signal for the worst case studied.

As for the laminar case, radial profiles in the turbulent flame show that CH exists only at the flame front, and its peak level decreases with increasing height above the burner. However, because of enhanced mixing from turbulence, the width of the CH peak is about two times wider than that for the laminar case at each height. For both flames, the CH peaks move outward with increasing distance above the burner owing to a greater flame diameter.

Representative time series for both the laminar (x/D=3) and turbulent (x/D=1) flames are shown in Figure 3. These measurements were obtained at the radial locations corresponding to the highest mean CH fluorescence signals. For the laminar flame, a post-filter was applied to the fluorescence signal to attenuate noise above 200 Hz. This filtering process enhanced the SNR so as to visually resolve the large scale pulsation in the flame caused by buoyancy. While the

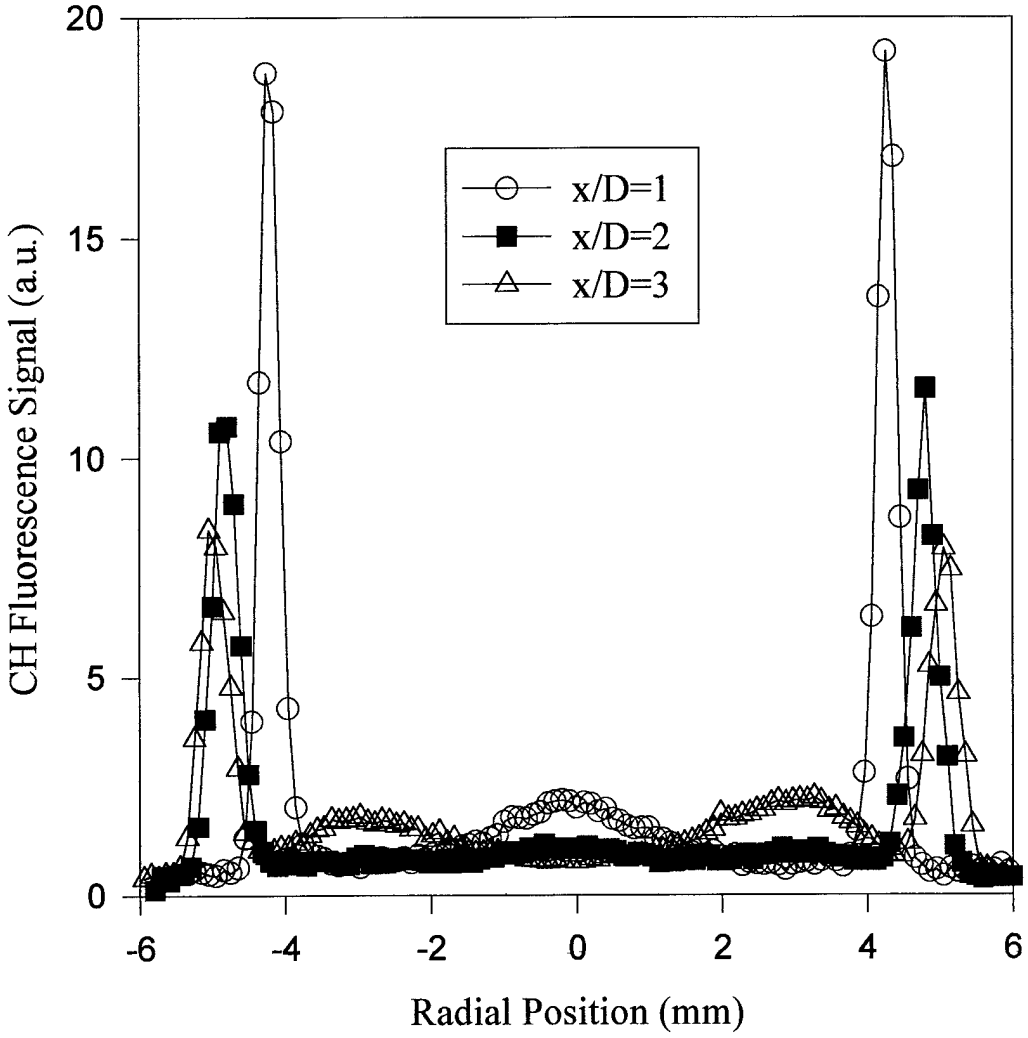

Figure 2. Mean CH signal measured in a laminar, methane/air, nonpremixed flame. Each data point represents the average of 1200 measurements. Curves are added to the measured data to aid the eye.

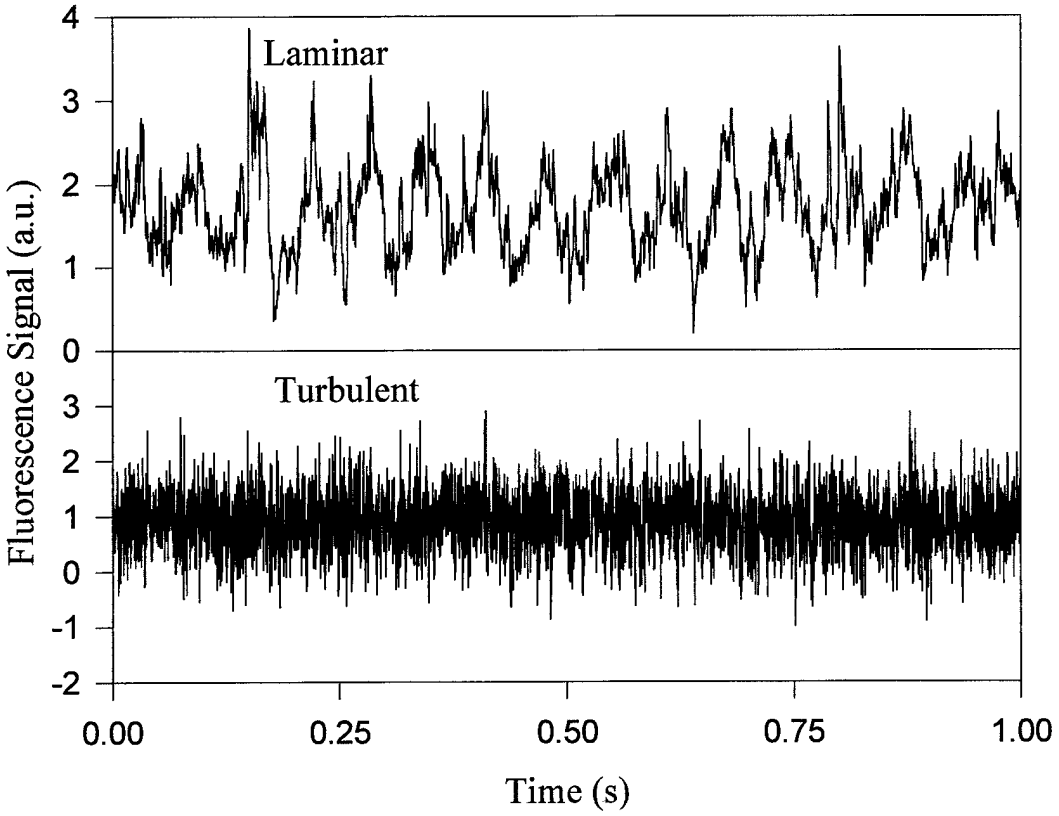

Figure 3. Representative CH time series for the laminar and the turbulent methane/air flames, showing 1 s of continuous data. The measurements were made at the radial location corresponding to the peak mean CH signal (laminar x/D=3; turbulent x/D=1).

turbulent time series contains many frequencies owing to turbulent fluctuations, no single, strong frequency is apparent as with the laminar time series.

Figure 4 shows PSDs generated from time-series measurements in both the laminar and turbulent flames. The PSDs were generated from data taken at the same axial and radial positions as presented in Fig. 3. The spectrum for the laminar flame is relatively flat, indicative of a steady flow. The spike at 16 Hz corresponds to the large-scale pulsation frequency for this flame (see Fig. 3). The spectrum from the turbulent flame shows the classic energy transfer found in turbulent flows. For locally-isotropic, turbulent flow at high Reynolds number, the spectrum of scalar fluctuations is expected to display a -5/3 power-law region [11]. As shown in Fig. 4, the spectrum does not follow this trend, instead displaying a decay coefficient of approximately -1.2. The relatively low Reynolds number for this turbulent flame may contribute to this difference [12].

2.4 OH Fluorescence Measurements

2.4.1 Laminar Flame Radial Profiles

Mean OH fluorescence radial profiles were measured in the same laminar flame at several heights above the burner, as shown in Fig. 5. The OH peak signal level does not change significantly with increasing height above the burner. The width of the OH peak, however, doubles from x=3 mm to x=30 mm and the location of the peaks moves farther out with increasing height because of flame widening. The width of the peak for OH is about twice that for CH owing to the existence of OH over a larger range of mixture fractions and temperatures [10]. Fluorescence detection spectra were obtained at several locations, and radial profiles were repeated after tuning the laser off the OH transition to check for potential interferences. Up to a height of x=30 mm, virtually all of the signal is from OH fluorescence. At x=40 mm and x=50 mm, significant interference occurs on the fuel side of the OH peak. The location and width of these interference peaks are very similar to those noted for the CH measurements and are likely caused by scattering from soot particles formed in the diffusion flame.

2.4.2 Laminar Flame Time Series and PSDs

Hydroxyl time series were obtained at selected radial locations in the laminar flame for several heights above the burner. In comparison to CH, OH measurements can be made at many heights and at radial locations away from the peak concentration. The fluorescence signal was sampled at 800 Hz for these measurements, thus resolving frequencies up to 400 Hz. Time series corresponding to radial peak concentrations were measured at heights of x=3, 10, and 30 mm. The PSDs computed from these time series are shown in Fig. 6. The low-frequency oscillation is apparent at each height, although the strength of the oscillation grows with increasing height above the burner, consistent with expectation [13]. In addition to this ~15-Hz frequency, components are present at 133 Hz owing to the chopper wheel rotation rate, 60 Hz owing to line noise, and 30 Hz for the measurement at x=30 mm. The latter component is likely a second harmonic of the buoyancy-induced flicker that is apparent as the amplitude becomes sufficiently large [13]. PSDs determined from measurements of OH in a laminar, premixed burner show only the 133-Hz and 60-Hz noise components. Other potential noise-sources (laser fluctuations, electronics, etc.) are below the shot-noise floor and do not contribute to the reported spectra.

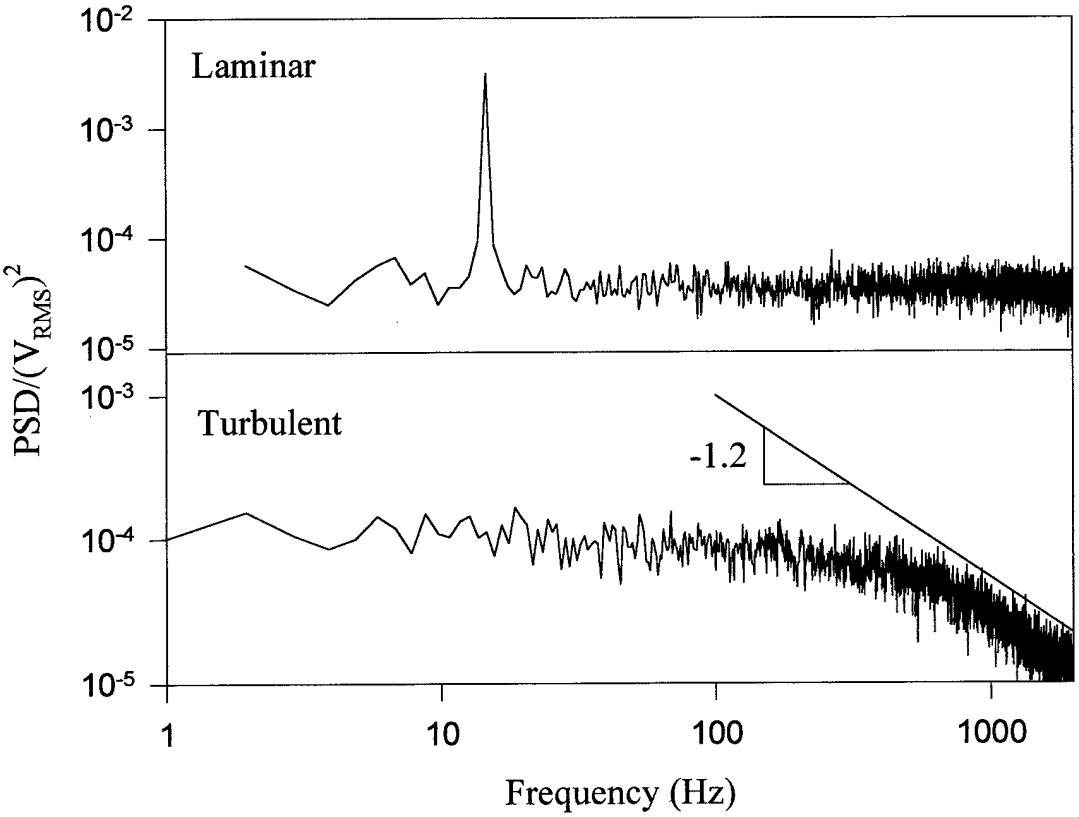

Figure 4. Power spectra corresponding to CH-fluorescence time series for the laminar and the turbulent methane/air flames. The measurement locations are the same as those in Fig. 3.

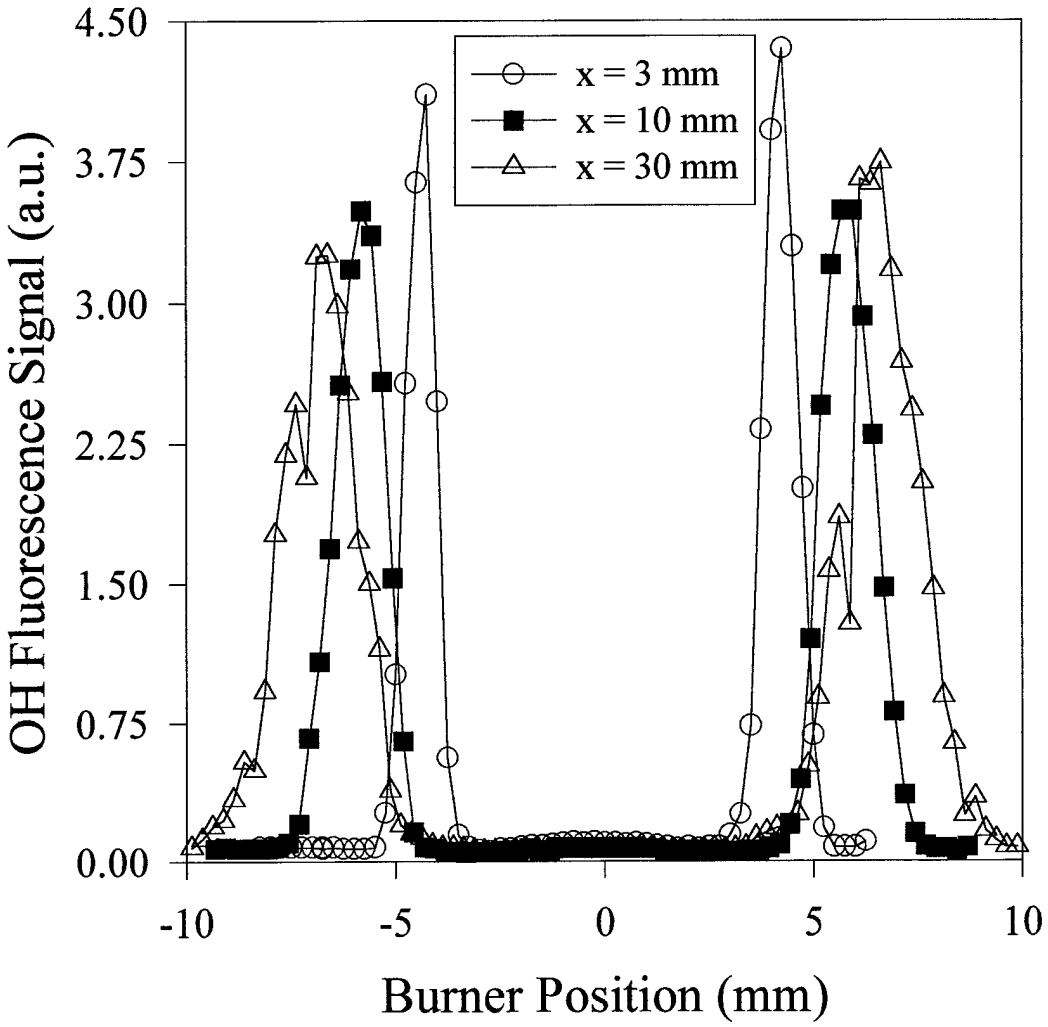

Figure 5. Mean, radial, OH-fluorescence profiles in the laminar diffusion flame.

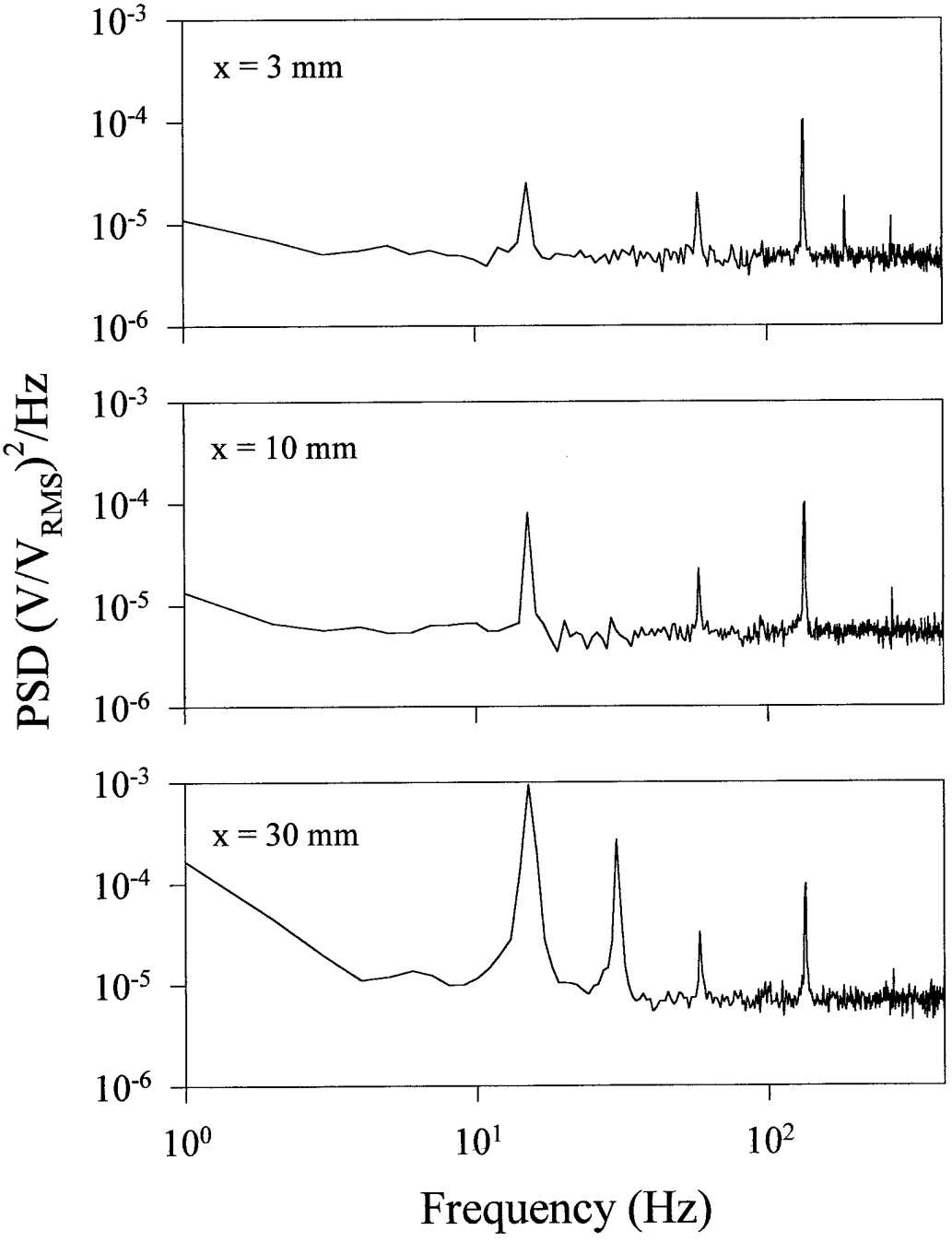

Figure 6. PSDs of OH-fluorescence signal in the flickering, laminar, diffusion flame. Fifty PSDs are averaged to obtain cleaner statistics.

Compared to the time series measured for CH, the SNR (mean/standard deviation) for OH is about ten times larger. The noise in the time series is largely caused by shot noise and by the ineffectiveness of the lock-in amplifier in measuring signals consisting of low average photon levels. The decrease in relative noise for OH results directly from an increase in the number of fluorescence photons reaching the PMT. An important consequence of this reduction in relative noise is a reduction in the PSD background. Ironically, this decrease in the noise floor causes the hydroxyl PSD to appear noisier than that for CH since small-amplitude noise sources (e.g., line noise) can now be resolved. If the noise floor from a typical CH time series were present for these OH measurements, even the buoyancy-induced frequency would not be apparent at the lowest measured height in Fig. 6.

A comparison between the CH and OH PSDs in this flame sheds light on another difference not caused by SNR issues. Comparing the amplitude of the buoyancy-induced fluctuation at 15 Hz, the CH PSD is observed to be two orders of magnitude greater than the OH PSD. The buoyancy forces cause a low-frequency oscillation of flame velocities [13]. The effect of this oscillation on the fluorescence time series arises from a convolution of these velocity fluctuations with the distribution in minor-species concentration. For OH, the concentration peaks are wider than those for CH in the radial direction and the changes in peak concentration are smaller than those for CH from one height to the next. The result is that a small amplitude velocity fluctuation will cause a small change in OH fluorescence signal, whereas this change is apparently much larger for CH. Likewise, measurements made at locations away from the concentration peak, where the concentration gradient is larger, should also show a stronger coupling between velocity and fluorescence fluctuations.

This postulated behavior with respect to the concentration gradient can be experimentally pursued by comparing time series and PSDs measured away from the radial peak. Time-series measurements of OH were made at the radial peak for x=5 mm and x=20 mm, and also 0.5 mm toward the fuel stream for x=5 mm. Figure 7 shows the corresponding PSDs for these three time series. A stronger coupling between the velocity fluctuation and the measured fluorescence fluctuation is observed at the location where the concentration gradient is largest for x=5 mm. The energy of the fluctuation is even larger for the off-peak case lower in the flame than for the on-peak case much higher in the flame, which underscores the importance of a greater concentration gradient. The noise floor for the off-peak measurement is also higher owing to the lower fluorescence signal. Thus, the PSD appears cleaner when in reality the spectral noise sources are just buried beneath a larger spectrally-uniform noise floor (shot-noise). This off-peak PSD is almost identical to that obtained at the radial peak concentration (x=3 mm) for CH.

2.4.3 Turbulent Flame Radial Profiles

Radial fluorescence profiles of OH were also measured in the turbulent flame (Re=2,800). As before, fluorescence detection spectra and off-resonance profiles were obtained to test for fluorescence interferences. No interferences were found below x=60 mm in this flame. As with CH, the radial profile is similar to that for the laminar flame except that the width is about twice that of the turbulent case. Unlike with CH, the SNRs achievable here permit a detailed examination of PSD and PDF shapes at different locations. PDFs are available with low repetition-rate lasers and as such are not unique to the PITLIF instrument; however, PDF and PSD shapes can now be compared for further analysis of such flames.

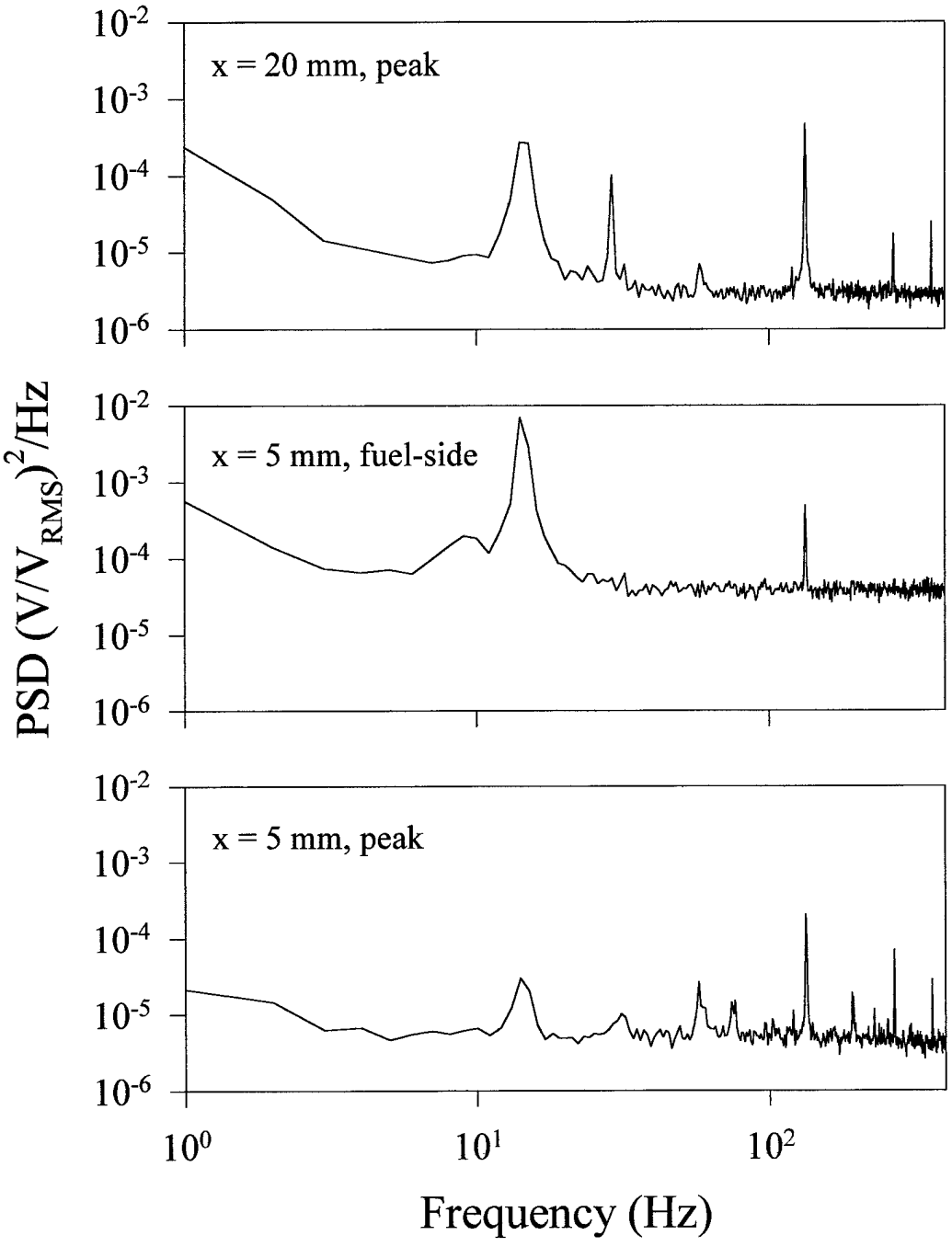

Figure 7. Hydroxyl PSDs comparing radial peak and fuel-side location measurements.

Time-series measurements were made at many radial locations at heights of x=5, 30, and 60 mm. The PDFs and PSDs for the x=30 mm and x=60 mm cases were found to be nearly identical to each other, but considerably different from the x=5 mm case. Consequently, a comparison is presented for only the x=5 and x=30 mm cases.

2.4.4 Turbulent Flame Probability Density Functions

Figure 8 shows the PDFs computed at x=30 mm for several radial locations. Far off the peak on either the air or fuel side (|y|>2 mm), the PDF is centered near zero (no measured signal). At these locations, there is still some deviation from the zero mean as a result of flame emission. At the radial peak, where the concentration is larger, the bulk of the PDF exists significantly above zero. However, even at the peak, fluctuations are large enough to cause a zero signal some of the time. The result is a bimodal structure in the PDF.

Figure 9 shows PDFs for x=5 mm at various radial locations. On the air side of the peak (y=0.5 mm), the PDF shows a nearly symmetric distribution toward higher and lower signals. At the peak, the PDF is again nearly symmetric. However, in this case, a long tail toward lower signals exists, but the probability is monotonically decreasing and not bimodal. A mirror image of the peak PDF occurs on the air side at y=1.0 mm. On the fuel side, the distribution is asymmetric, skewed in one direction or the other depending on the mean value. For the symmetric PDFs, the signal does not always contain zero values (e.g. the air-side PDF at y=0.5 mm in Fig. 9), particularly for the larger mean signal locations, whereas for the skewed (bimodal) PDFs, the probability of obtaining no signal is always greater than zero and often represents a significant portion of the overall time series.

Comparing the two heights, the PDF shape for x=30 mm does not significantly change from the air side to the fuel side. The distribution is sometimes less bimodal than at the peak (y=0 mm), but it is always asymmetric, and all differences are likely a result of only the changing mean concentration. In contrast, the PDF shape at x=5 mm is asymmetric on the fuel side (similar to all PDFs at x=30 mm) and symmetric on the air side. This difference cannot be described by just a change in the mean concentration. Since the flame is attached to the burner, the scalar fluctuations are attenuated at lower elevations (x=5 mm) and grow downstream [13]. This effect could impact both the PDFs and PSDs. Moreover, at the lower heights, the flame front is outside the shear layer [14]; thus, the impact of fuel-stream turbulence on species concentration could be more important for fuel-side measurements than for air-side measurements, which may be dominated by the buoyant outer flow [13]. Higher in the flame, where both the shear layer and the scalar fluctuations are greater, the differences from the air side to the fuel side should be less pronounced, as found in our experimental measurements.

2.4.5 Turbulent Flame Power Spectral Densities

PSDs were also computed at each of the points corresponding to the previous PDFs. Figure 10 shows the PSDs at x=30 mm. Each PSD appears to have a two-slope structure with a linear region (log-log scale) from DC to ~100 Hz and a second linear region above ~200 Hz. The second slope decays into the noise floor, which is a function of the SNR. Consistent with the PDFs (Fig. 8), no substantial difference is observed from the fuel to the air side. The fuel-side PSD has a slightly higher knee frequency (intersection of first and second slopes), and the transition from one slope to the next is sharper, but these differences are small. From linear fits

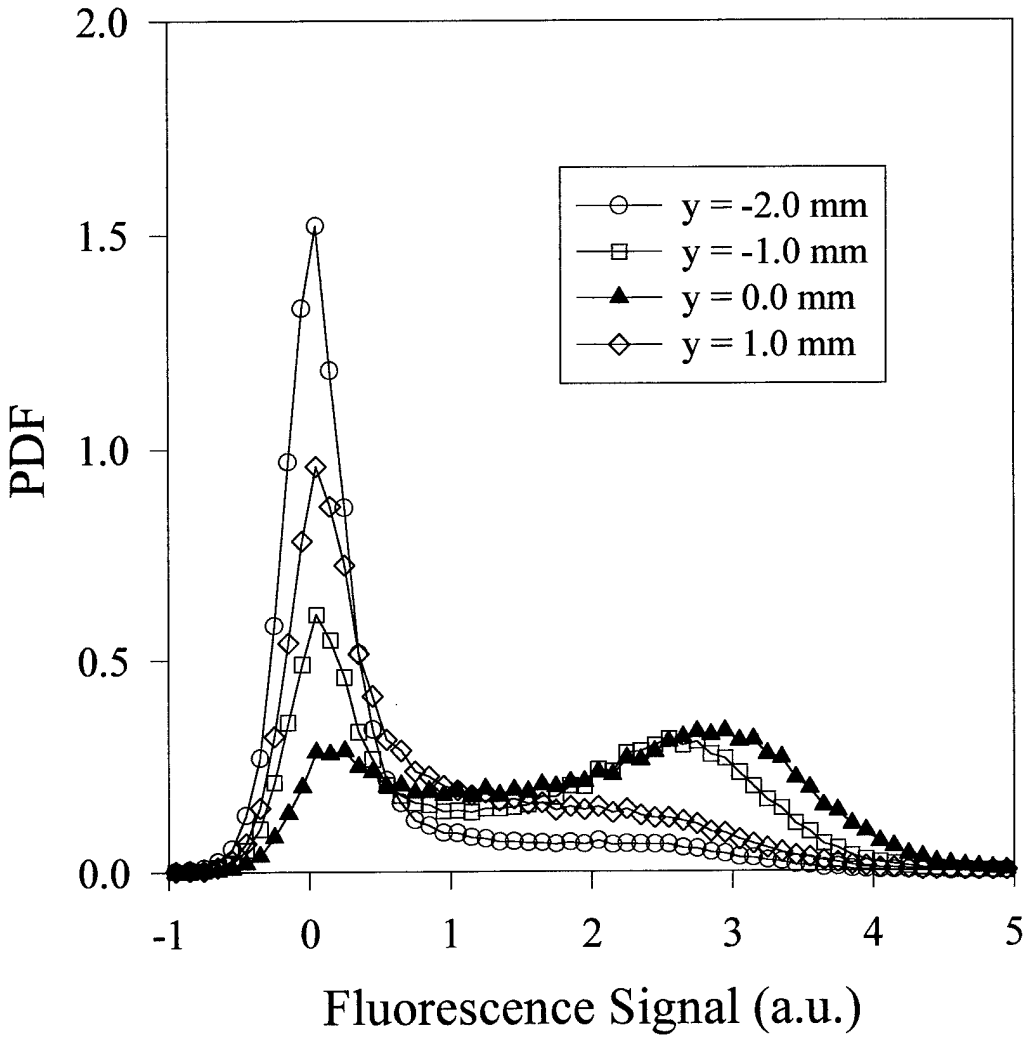

Figure 8. Hydroxyl PDFs measured at x=30 mm in the turbulent diffusion flame for various radial locations (y). Negative values of y are on the fuel side of the peak (0 mm).

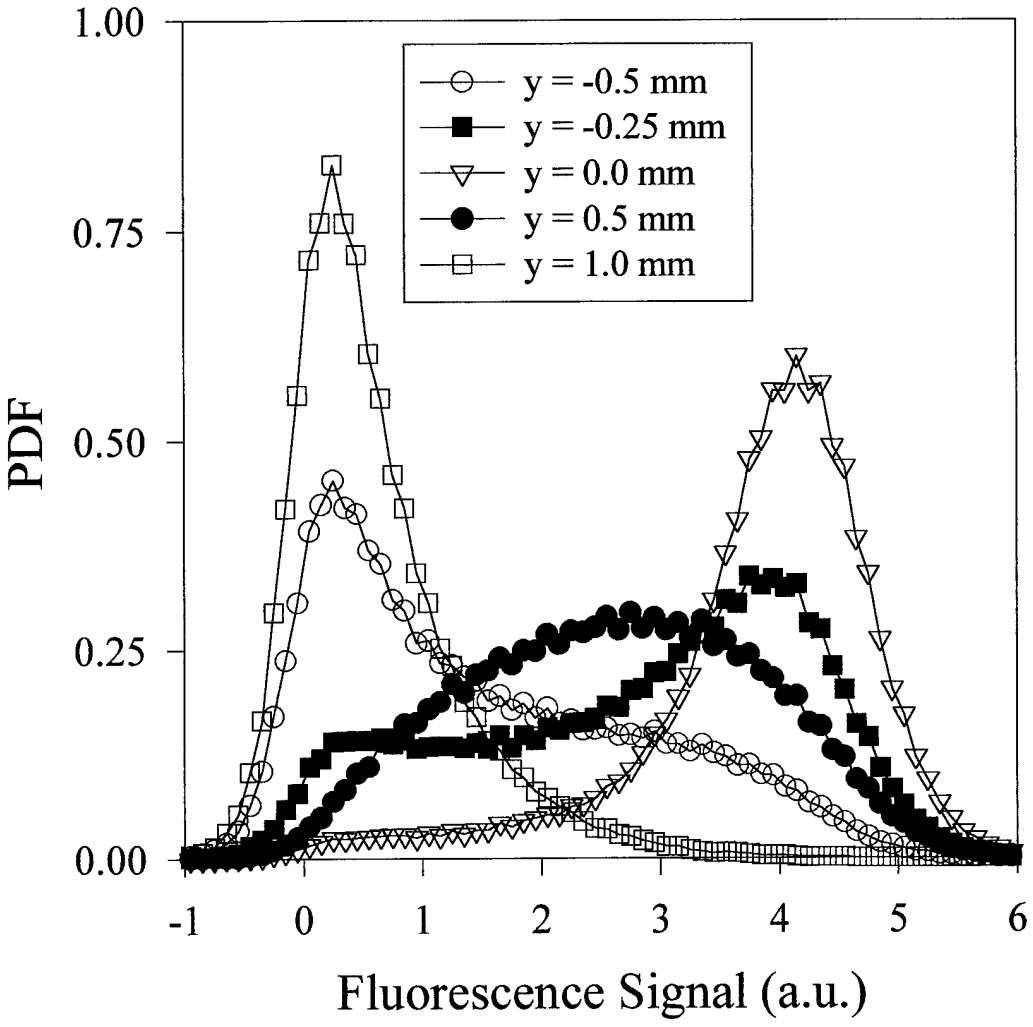

Figure 9. Hydroxyl PDFs measured at x=5 mm in the turbulent diffusion flame as a function of radial position (y). Negative values of y are on the fuel side of the radial peak (0 mm).

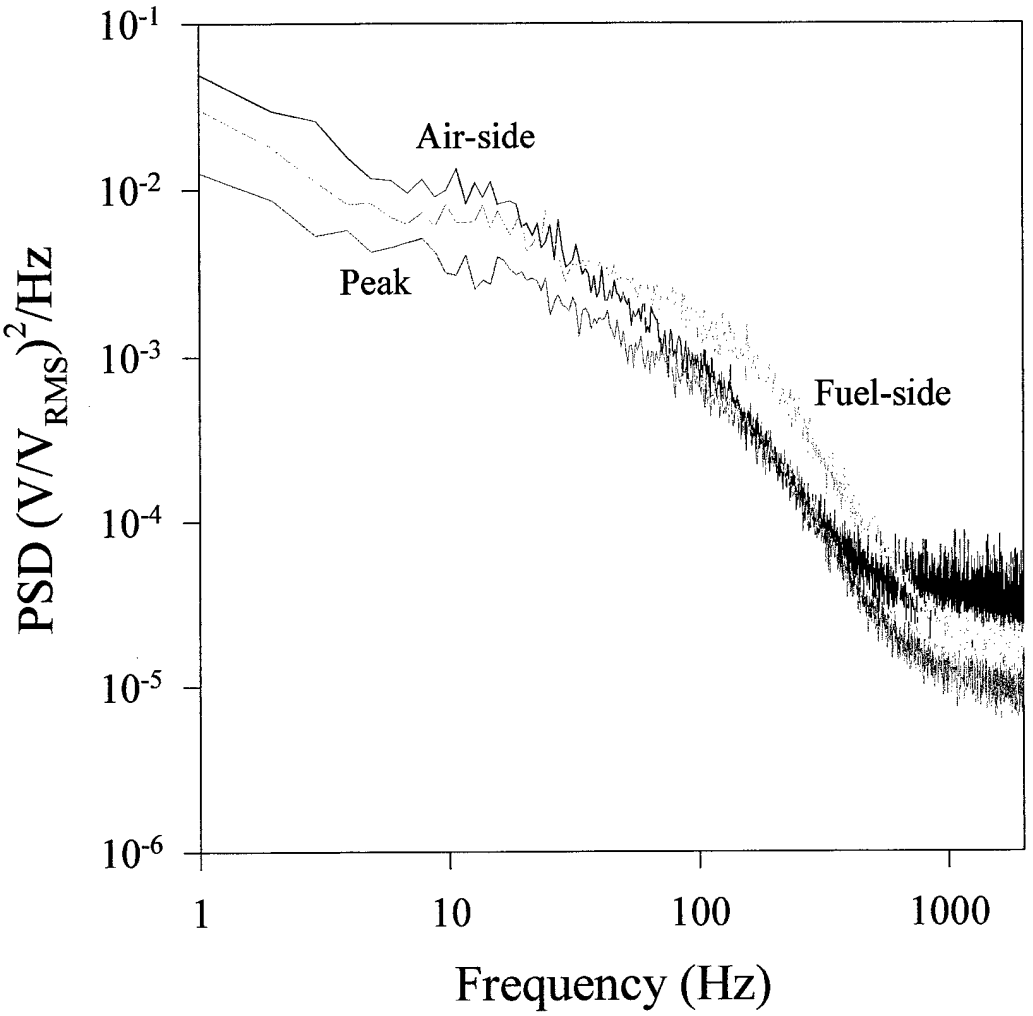

Figure 10. Hydroxyl PSDs measured at x=30 mm in the turbulent diffusion flame. The darkest line is 1.0 mm to the air side of the peak, the medium line is at the peak, and the lightest line is 1.5 mm to the fuel side of the peak.

to these two slopes, the decay coefficient for the first slope varies from about -0.5 to -1.0 from the fuel to the air side, respectively. The second (high-frequency) slope does not vary significantly from the fuel to the air side, having an average value of about -2.4. The uncertainty in this slope is about 15% for the measurements from one side to the other. Some of this difference arises from the need to vary the fit range as the knee frequency changes or as the noise floor rises, which begins to corrupt the higher frequency regions. A repeatability analysis reveals an uncertainty (95% confidence interval) of less than 5% in this slope for measurements repeated at the same location, for which the knee frequency and noise floor remain constant.

Figure 11 shows a similar comparison of PSDs for a height of x=5 mm. At this height, significant differences are found from the fuel to the air side, similar to the PDFs (Fig. 9). The fuel-side PSD has a two-slope structure with a sharp transition between the first and second linear slope. As at x=30 mm, the knee frequency decreases from the fuel to the air side of the flame front. For the air-side PSD, the two slopes are so close in magnitude that the PSD visually looks like a single-slope decay. The low frequency slope varies again from about -0.5 to -1.0 from the fuel to the air side, respectively. The high-frequency slope is approximately -2.2 for the fuel-side PSD, and drops to about -1.2 for the air-side PSD.

Recall that the CH PSD was previously found to display a slope of -1.2 for both fuel- and air-side measurements. This slope is nearly identical to that for the OH measurement on the air side at the same height, despite the significantly narrower radial distribution of CH. However, the OH fluctuations are much higher in amplitude at lower frequencies. Since the measurements are not made at the same radial location, the similarities could be coincidental. Moreover, at this low height, the overall standard deviation of the hydroxyl time-series measurement is not significantly greater than the maximum possible fluctuation from electronic quenching (±15%). Thus, the effects of quenching could be problematic to measurements in this region of the flame. In particular, some of the disparity between the OH and CH PSDs could be a result of differences in quenching fluctuations.

Some OH measurements were also made below x=5 mm. As the probe volume approaches the burner surface, vignetting becomes problematic, and the radial profile cannot be adequately characterized. Nevertheless, the PSDs measured very near the burner surface (x=1 mm) were found to be identical from the fuel to the air side, each having a single-slope structure with a slope of about -1.2 above around 10 Hz. Moreover, the PDFs at these locations were found to be symmetric at all radial measurement locations.

2.4.6 Interpretation of Turbulent Flame Results

The possible significance of a PSD slope steeper than -2.0 can be addressed by examining the relationship between velocity fluctuations and the fluorescence signal via the radial shape of the hydroxyl profile. Momentarily neglecting other sources of potential fluorescence fluctuations (quenching variations, diffusion, and OH creation or depletion) and assuming that all variations result from velocity fluctuations, which merely move the OH radial profile back and forth across the probe volume, a relationship can be found between the velocity and fluorescence PSDs. Under these assumptions, the instantaneous fluorescence signal can only be a function of the instantaneous position of the radial OH profile. Consequently, the fluorescence time series must be proportional to the integral of the velocity time series.

The relationship between the spectrum of a function (position, x) as compared to its derivative (velocity, v) is well known [15, 11], i.e.,

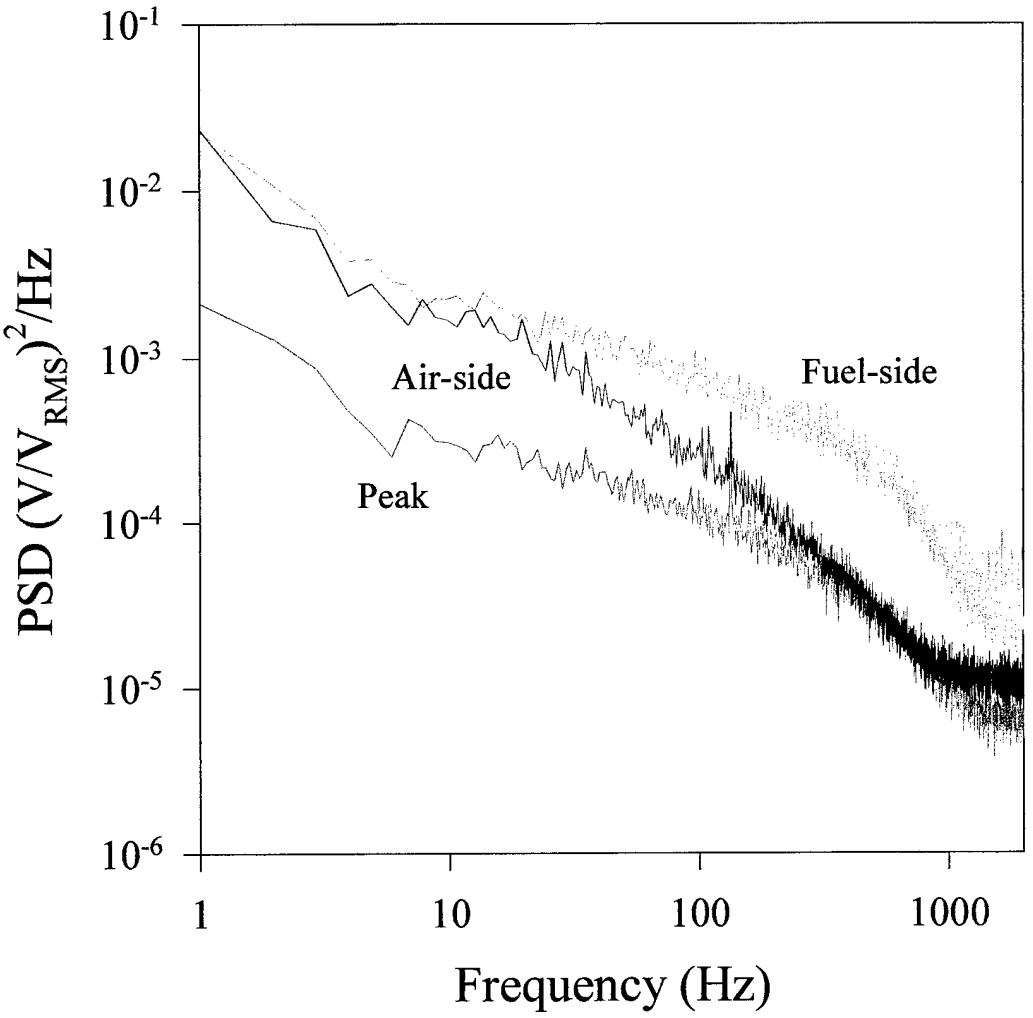

Figure 11. Hydroxyl PSDs measured at x=5 mm in the turbulent diffusion flame. The darkest line is 0.5 mm to the air side of the peak, the medium line is at the peak, and the lightest line is 0.5 mm to the fuel side of the peak.

$$S_v(\omega) = \omega^2 S_x(\omega). \quad (1)$$

This equation implies that the OH-fluorescence spectrum will have an additional -2.0 slope imposed upon that for the velocity spectrum but will otherwise maintain the same shape. If the above effect, namely convection of the radial OH profile without a change in its basic shape, is to be the dominant or only source of fluctuations, the slope of the PSD must be steeper than -2.0 at high frequencies, as the velocity PSD in turbulent flames is most likely itself decaying at a significant slope. Fluorescence PSDs with slopes steeper than -2.0 are very possibly dominated at high frequencies by this velocity effect, although many other physical processes are occurring, such as electronic quenching, diffusion, and reaction. A possibility for future work in this area is to compare fluorescence and velocity PSDs obtained at the same point in the flame.

The present analysis implicitly assumes that the fluorescence time series accurately mimics the time series for flame location. This assumption is most accurate for small-scale fluctuations (high frequencies) which do not encompass a large portion of the OH spatial distribution. For large-scale fluctuations, we must obviously consider the convolution of the actual radial profile with the greater fluctuations in flame-front location.

For many PSDs measured in the turbulent diffusion flame ($x \geq 5$ mm), the high-frequency slopes are near -2.4. If the above convective effect were responsible, this value would indicate a velocity decay with a slope of only -0.4. This slope is far below the Kolmogorov limited -5/3, but the Reynolds number for our flame is also very low, and a strong dependence of the high-frequency slope on Reynolds number has been observed in previous velocity measurements [16]. For the case of a fixed scalar profile moving across the measurement location, the PDF can be estimated from an assumed, Gaussian velocity PDF [17] and can result in a bimodal shape [18]. The bimodal or skewed PDFs measured here match the types of PDFs computed by Effelsberg and Peters [17]. Furthermore, the bimodal PDFs in the current investigation coincide with PSD slopes steeper than -2.0 in all cases. Additional sources for these fluctuations should be examined in future work, but both the PDFs and PSDs measured high in the turbulent diffusion flame are consistent with fluctuations associated only with convection. This simplification is consistent with neglecting the diffusion and reaction rate terms in the species conservation equation. Neglecting w_i is equivalent to assuming that the species concentration, Y_i, is only a function of a conserved scalar; that is, both Y_i and the mixture fraction are governed by the same conservation equation.

For locations where the PDF appears Gaussian, the high-frequency slope of the PSD is around -1.2 in most cases. This slope is insufficiently steep to be described solely by convection. The relevant regions are low in the diffusion flame, where the flame is attached to the burner. In these regions the scalar dissipation rate is much higher [19], and neglecting source terms when evaluating fluctuating species likely becomes invalid. Minor-species concentrations are not generally well described by just the mixture fraction [20], so this behavior is not unexpected. The PSDs for other species and temperature (as required to calculate w_i) may need to be considered to describe the hydroxyl PSDs in these regions. Velocity time series measured at the same point in the flame could be used with composition and temperature profiles and simplified chemistry to attempt a calculation of OH and CH PSDs. For now, without these measurements, hydroxyl PSDs can only be compared to other time-resolved scalar measurements in similar flames.

McQuay and Cannon [21] recently measured temperature PSDs in an elliptic diffusion flame (Re=6,000). Although much of their work was focused on the differences occurring on the major and minor axes of these flames, the PSDs are some of the most detailed found in the

literature. The temperature PSDs are characterized by slopes similar to those measured for OH. In particular, the fuel-side temperature PSDs are flat at low frequencies, show a sharp knee frequency at several hundred Hertz, and display a power-law decay at higher frequencies with slopes steeper than -2.0. Moving toward the air side, the knee frequency decreases, and the transition between the flat, low-frequency and decaying, high-frequency regions becomes less clear. Finally, far on the air side, the PSDs are characterized by one slope over nearly all relevant frequencies. High in the flame, the temperature PSDs are more similar from the air to the fuel side. The associated PDFs are also largely asymmetric, although never bimodal. The existence of enhanced, small-scale fluctuations in the fuel stream for both temperature and OH is consistent with the numerical predictions of Katta and Roquemore [14]. However, unlike the present OH measurements, the high-frequency slopes of McQuay and Cannon [21] are always steeper than -2.0. This slope is consistent with convection-dominated fluctuations for temperature. Low in the flame, where the hydroxyl PSDs appear to indicate that non-convective terms are important, the temperature PSDs still exceed -2.0.

2.4.7 Hydrogen/Argon Turbulent Diffusion Flames

Finally, we present more recent PITLIF measurements in a turbulent, hydrogen/argon/air, diffusion flame to illustrate the effect of Reynolds number on the OH spectra. The fuel was a mixture of 78% hydrogen and 22% argon by volume. The flow rate of the mixture was varied to give Reynolds numbers from 2,800 to 17,000. The burner used was the same as that for the low Reynolds number, methane/air studies (5.5-mm diameter tube).

Figure 12 shows the experimentally determined PSDs for Re=2,800, 9,000, and 17,000 at a single height in the flame. The high-frequency slopes determined by a least-squares fit to the range 100-500 Hz are -1.72, -0.70, and -0.26 for the three cases, respectively. Each time-series measurement was taken at the radial location of maximum fluorescence signal for an axial location of 110 mm above the burner surface. A laminar-flamelet based simulation was performed to examine the relationship between mixture-fraction fluctuations and minor-species-concentration fluctuations. The evolution of the experimental PSDs from low to high Reynolds number qualitatively matches simulations of the evolution from low to high fluctuation intensity in mixture fraction. Several difficulties currently limit our ability to compare, quantitatively, these measured PSDs to the simulations. As discussed earlier, the measurements are not completely independent of the electronic quenching rate coefficient. Moreover, the noise floor is a result of the relatively low SNR. Our continuing work with the experimental aspects of this research is focussing on correcting for both of these difficulties.

A comparison of OH PSDs measured high in the methane flame to those measured high in the hydrogen/argon flame at a similar Reynolds number (Re=2,800) shows remarkable agreement. Both the low-frequency and high-frequency slopes for these PSDs match almost exactly. This agreement is only achieved relatively high in the flame where the assumption of convection-dominated fluctuations is most likely to be valid. Future work with mixture-fraction modeling of these PSDs should focus on this region for both flames.

3 CONCLUSIONS

CH and OH fluorescence time series have been obtained in both laminar and turbulent diffusion flames for the first time. Unfortunately, the current state of the electronics used with

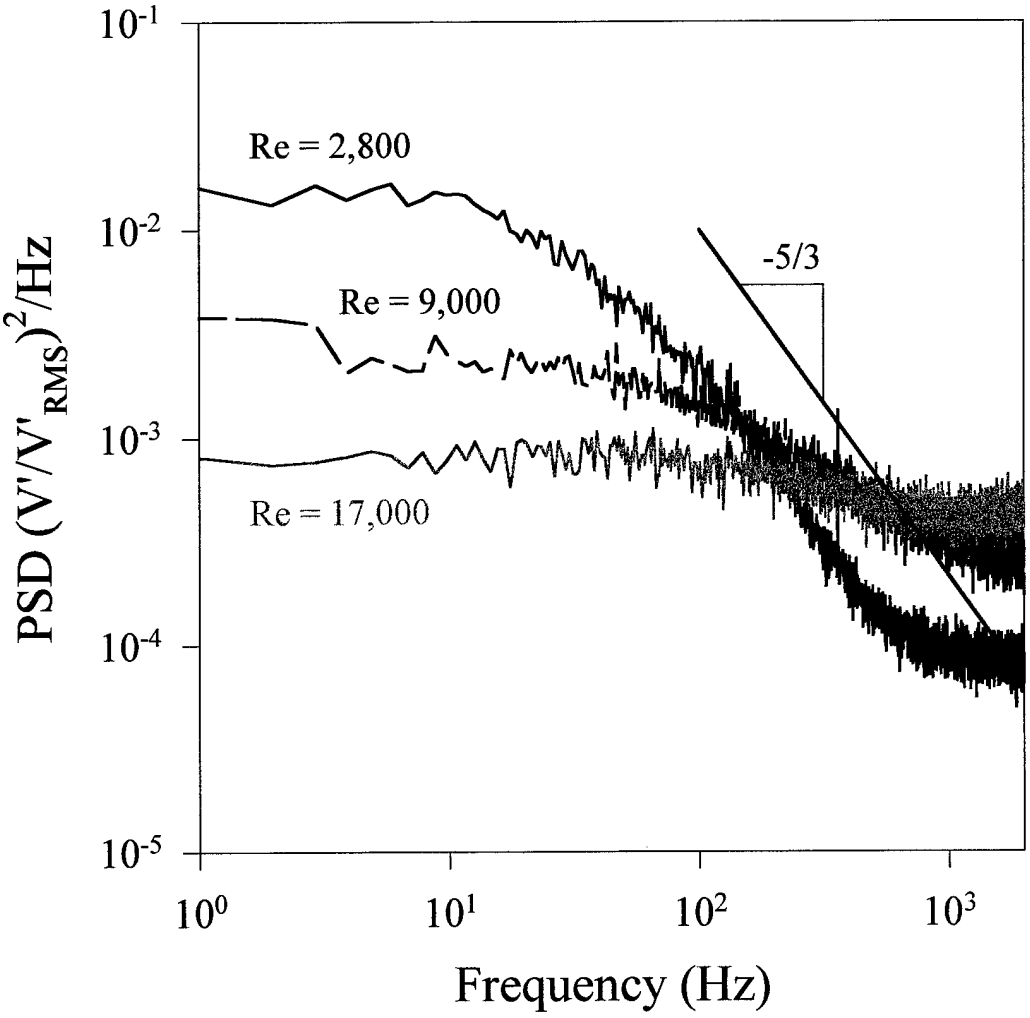

Figure 12. Experimental OH PSDs measured at an axial height of 110 mm in a 78% hydrogen/22% argon, diffusion flame. Measurements are made at the radial location of peak fluorescence signal.

the PITLIF instrument does not allow real-time quenching corrections to the measured time series, which is recognized as a potential limitation to the current measurements. Present work on an associated AASERT grant is involved in upgrading the electronics to allow on-the-fly quenching corrections. However, estimates for the variations in CH and OH quenching rate coefficients in a diffusion flame show that the associated error should be less than ±25% and ±15%, respectively. Thus, the time series reported still represent species concentrations up to this limit. Moreover, the PDFs and PSDs computed from the PITLIF measurements have sufficient SNRs to provide detailed information at a variety of locations in both laminar and moderately-turbulent flames. The application of PITLIF to hydrogen/argon flames at higher Reynolds numbers shows for the first time the evolution of minor-species PSDs through the transition regime and into fully-turbulent flow. These flames should allow future work to focus on fully-turbulent conditions.

The significant results of the present study can be summarized as follows:

1) The laminar flame displays a strong ~15-Hz, buoyancy-induced, CH- and OH-fluorescence oscillation.
2) The strength of this oscillation in the PSD depends on the local concentration gradient.
3) Hydroxyl PSDs measured high in the turbulent diffusion flame are found to have high-frequency slopes steeper than -2.0, possibly a result of convective fluctuations.
4) Low in the turbulent diffusion flame, the CH and OH PSDs display slopes very close to -1.2, which is not steep enough to be described by pure convective fluctuations.
5) PSDs measured on the fuel side of the turbulent flame front are characterized by more intense small-scale (high-frequency) fluctuations than those on the air side. This behavior is consistent with other scalar (temperature) measurements in similar flames [21] and with numerical predictions [14].
6) PDFs at all locations where the PSD slope is steeper than -2.0 are asymmetric and usually bimodal. This behavior can be predicted from turbulent PDF analysis [18] and is consistent with previous scalar measurements of temperature [22] and density [23]. Both the steep PSD slope and the bimodal PDF shape can be derived from the species-conservation equation if all fluorescence fluctuations are assumed to arise from convection.
7) Measurements of OH in hydrogen/argon diffusion flames shows that the fluorescence PSD becomes less steep with increasing Reynolds number. This trend qualitatively matches simulations of fluorescence PSDs performed using a laminar-flamelet analysis.

In general, the PSDs measured are very repeatable and display interesting similarities and differences when compared with other scalar measurements. The present analysis suggests that regions high in diffusion flames at low Reynolds numbers may be sufficiently dominated by species convection that chemical reaction rates might not be needed to describe relevant OH fluctuations. This simplification would be equivalent to treating [OH] as solely a function of the local mixture fraction (as in our PSD simulations). However, regions low in the flame, where primary oxidation of the fuel is occurring, apparently cannot be treated in this relatively simple manner.

In summary, we have demonstrated PITLIF's capability for monitoring minor-species fluctuations in real time at rates sufficiently rapid to permit the study of transient events in practical combustion environments. The PITLIF technique has the potential to provide valuable experimental information not previously available concerning minor-species concentrations. This information can be used to examine the accuracy of models which treat these flames, and to

study the frequency content of turbulent fluctuations for minor-species concentrations as compared to other scalars in the flow field.

4 PERSONNEL AND TECHNOLOGY TRANSFERS

Professors Galen B. King and Normand M. Laurendeau are co-principal investigators for this research program. Mr. Michael W. Renfro is a continuing Ph.D. student on the research team. Mr. Spencer D. Pack will complete his M.S. program during the upcoming summer. Mr. Arvind Lakshmanarao joined the project as a new M.S. student in August, 1997.

Plans are underway for a joint effort with Dr. James Gord at Wright-Patterson Air Force Base. Experiments using both PITLIF and ASOPS are possible.

5 PUBLICATIONS AND PRESENTATIONS

(1) Klassen, M. S., Renfro, M. W., King, G. B., Laurendeau, N. M., Time-series measurements of CH in turbulent non-premixed CH_4/air flames. Central States Section Meeting, The Combustion Institute, St. Louis, MO (1996).

(2) Renfro, M. W., Klassen, M. S., King, G. B., Laurendeau, N. M., Time-series measurements of CH concentration in turbulent CH_4/air flames by use of picosecond time-resolved laser-induced fluorescence. *Optics Letters* 22:175-177 (1997).

(3) Renfro, M. W., Pack, S. D., King, G. B., Laurendeau, N. M., Hydroxyl time-series measurements in laminar and turbulent methane/air diffusion flames. Spring Meeting, Western States Section, The Combustion Institute, Livermore, CA (1997).

(4) Renfro, M. W., Time-series measurements of laser-induced OH and CH fluorescence in laminar and turbulent flames. M.S. Thesis, Purdue University, West Lafayette, IN (1997).

(5) Laurendeau, N. M., Application of picosecond time-resolved laser-induced fluorescence to CH and OH measurements in laminar and turbulent flames. Invited presentation, Gordon Research Conference on *The Physics and Chemistry of Laser Diagnostics in Combustion*, Plymouth, NH (1997).

(6) Renfro, M. W., Pack, S. D., King, G. B., Laurendeau, N. M., Hydroxyl time-series measurements in turbulent diffusion flames. Gordon Research Conference on *The Physics and Chemistry of Laser Diagnostics in Combustion*, Plymouth, NH (1997).

(7) Renfro, M. W., Pack, S. D., King, G. B., Laurendeau, N. M., Hydroxyl time-series measurements in laminar and turbulent methane/air diffusion flames. *Combustion and Flame*, in press (1998).

(8) Renfro, M. W., Sivathanu, Y. R., Gore, J. P., King, G. B., Laurendeau, N. M., Time-series analysis and measurements of intermediate species concentration spectra in turbulent nonpremixed flames. *Twenty-Seventh International Symposium on Combustion*, Boulder, CO, in review (1998).

6 REFERENCES

1. Drake, M. C. and Pitz, R. W., *Exp. Fluids* 3:283 (1985).
2. Klassen, M. S., Thompson, B. D., Reichardt, T. A., King, G. B., and Laurendeau, N. M., *Combust. Sci. and Tech.* 97:391 (1994).
3. Reichardt, T. A., Klassen, M. S., King, G. B., and Laurendeau, N. M., *Appl. Opt.* 35:2125-2139 (1996).
4. Norton, T. S. and Smyth, K. C., *Combust. Sci. and Tech.* 76:1 (1991).
5. Cattolica, R. J., Stepowski, D., Puechberty, D., and Cottereau, M., *J. Quant. Spectrosc. Radiat. Transfer* 32:363 (1984).
6. Smyth, K. C., and Tjossem, P. J. H., *Appl. Phys. B* 50:499-511 (1990).
7. Sivathanu, Y. R., and Faeth, G. M., *Combust. Flame* 82:211-230 (1990).
8. Paul, P. H., *J. Quant. Spectrosc. Radiat. Transfer* 51:511-524 (1994).
9. Barlow, R. S., and Carter, C. D., *Combust. Flame* 97:261-280 (1994).
10. Smooke, M. D., Xu Y., Zurn, R. M., Lin, P., Frank, J. H., and Long, M. B., *Twenty-fourth Symposium (International) on Combustion*, The Combustion Institute, Pittsburgh, 1992, pp. 813-821.
11. Tennekes, H., and Lumley, J. L., *A First Course in Turbulence*, The MIT Press, Cambridge, MA, 1972.
12. Dowling, D. R. and Dimotakis, P. E., *J. Fluid Mech.* 218:109 (1990).
13. Chen, L. -D., Seaba, J. P., Roquemore, W. M., and Goss, L. P., *Twenty-second Symposium (International) on Combustion*, The Combustion Institute, Pittsburgh, 1988, pp. 677-684.
14. Katta, V. R., and Roquemore, W. M., *Combust. Flame* 92:274-282 (1993).
15. Kreyszig, E., *Advanced Engineering Mathematics*, 7th ed., John Wiley & Sons, Inc., New York, 1993.
16. Mydlarski, L., and Warhaft, Z., *J. Fluid Mech.* 320:331-368 (1996).
17. Effelsberg, E., and Peters, N., *Combust. Flame* 50:351-360 (1983).
18. Peters, N., *Twenty-first Symposium (International) on Combustion*, The Combustion Institute, Pittsburgh, 1986, pp. 1231-1250.
19. Effelsberg, E., and Peters, N., *Twenty-second Symposium (International) on Combustion*, The Combustion Institute, Pittsburgh, 1988, pp. 693-700.
20. Smyth, K. C., Miller, J. H., Dorfman, R. C., Mallard, W. G., and Santoro, R. J., *Combust. Flame* 62:157-181 (1985).
21. McQuay, M. Q., and Cannon, S. M., *Combust. Sci. and Tech.* 119:13-33 (1996).
22. Dibble, R. W., and Hollenbach, R. E., *Eighteenth Symposium (International) on Combustion*, The Combustion Institute, Pittsburgh, 1981, pp. 1489-1499.
23. Bill, Jr., R. G., Namer, I., and Talbot, L., *Combust. Flame* 44:277-285 (1982).